12

CASE STUDIES

In this chapter, we present three case studies which illustrate a number of important practical issues, namely: weights selection in $\mathcal{H}_\infty$ mixed-sensitivity design, disturbance rejection, output selection, two degrees-of-freedom $\mathcal{H}_\infty$ loop-shaping design, ill-conditioned plants, μ analysis and μ synthesis.

12.1 Introduction

The complete design process for an industrial control system will normally include the following steps:

1. *Plant modelling:* to determine a mathematical model of the plant either from experimental data using identification techniques, or from physical equations describing the plant dynamics, or a combination of these.
2. *Plant input-output controllability analysis:* to discover what closed-loop performance can be expected and what inherent limitations there are to 'good' control, and to assist in deciding upon an initial control structure and may be an initial selection of performance weights.
3. *Control structure design:* to decide on which variables to be manipulated and measured and which links should be made between them.
4. *Controller design:* to formulate a mathematical design problem which captures the engineering design problem and to synthesize a corresponding controller.
5. *Control system analysis:* to assess the control system by analysis and simulation against the performance specifications or the designer's expectations.
6. *Controller implementation:* to implement the controller, almost certainly in software for computer control, taking care to address important issues such as anti-windup and bumpless transfer.
7. *Control system commissioning:* to bring the controller on-line, to carry out on-site testing and to implement any required modifications before certifying that the controlled plant is fully operational.

In this book we have focused on steps 2, 3, 4 and 5, and in this chapter we will present three case studies which demonstrate many of the ideas and practical techniques which can be used in these steps. The case studies are not meant to produce the 'best' controller for the application considered but rather are used here to illustrate a particular technique from the book.

In case study 1, a helicopter control law is designed for the rejection of atmospheric turbulence. The gust disturbance is modelled as an extra input to an S/KS $\mathcal{H}_\infty$ mixed-sensitivity design problem. Results from nonlinear simulations indicate significant improvement over a standard S/KS design. For more information on the applicability of $\mathcal{H}_\infty$ control to advanced helicopter flight, the reader is referred to Walker and Postlethwaite (1996) who describe the design and ground-based piloted simulation testing of a high performance helicopter flight control system.

Case study 2 illustrates the application and usefulness of the two degrees-of-freedom $\mathcal{H}_\infty$ loop-shaping approach by applying it to the design of a robust controller for a high performance areo-engine. Nonlinear simulation results are shown. Efficient and effective tools for control structure design (input-output selection) are also described and applied to this problem. This design work on the aero-engine has been further developed and forms the basis of a multi-mode controller which has been implemented and successfully tested on a Rolls-Royce Spey engine test facility at the UK Defence Research Agency, Pyestock (Samar, 1995).

The final case study is concerned with the control of an idealized distillation column. A very simple plant model is used, but it is sufficient to illustrate the difficulties of controlling ill-conditioned plants and the adverse effects of model uncertainty. The structured singular value μ is seen to be a powerful tool for robustness analysis.

Case studies 1, 2 and 3 are based on papers by Postlethwaite et al. (1994), Samar and Postlethwaite (1994), and Skogestad et al. (1988), respectively.

12.2 Helicopter control

This case study is used to illustrate how weights can be selected in $\mathcal{H}_\infty$ mixed-sensitivity design, and how this design problem can be modified to improve disturbance rejection properties.

12.2.1 Problem description

In this case study, we consider the design of a controller to reduce the effects of atmospheric turbulence on helicopters. The reduction of the effects of gusts is very important in reducing a pilot's workload, and enables aggressive manoeuvers to be carried out in poor weather conditions. Also, as a consequence of decreased

buffeting, the airframe and component lives are lengthened and passenger comfort is increased.

The design of rotorcraft flight control systems, for robust stability and performance, has been studied over a number of years using a variety of methods including: H_∞ optimization (Yue and Postlethwaite, 1990; Postlethwaite and Walker, 1992); eigenstructure assignment (Manness and Murray-Smith, 1992; Samblancatt et al., 1990); sliding mode control (Foster et al., 1993); and H_2 design (Takahashi, 1993). The H_∞ controller designs have been particularly successful (Walker et al., 1993), and have proved themselves in piloted simulations. These designs have used frequency information about the disturbances to limit the system sensitivity but in general there has been no explicit consideration of the effects of atmospheric turbulence. Therefore by incorporating practical knowledge about the disturbance characteristics, and how they affect the real helicopter, improvements to the overall performance should be possible. We will demonstrate this below.

The nonlinear helicopter model we will use for simulation purposes was developed at the Defence Research Agency (DRA), Bedford (Padfield, 1981) and is known as the Rationalized Helicopter Model (RHM). A turbulence generator module has recently been included in the RHM and this enables controller designs to be tested on-line for their disturbance rejection properties. It should be noted that the model of the gusts affects the helicopter equations in a complicated fashion and is self contained in the code of the RHM. For design purposes we will imagine that the gusts affect the model in a much simpler manner.

We will begin by repeating the design of Yue and Postlethwaite (1990) which used an S/KS $\mathcal{H}_\infty$ mixed sensitivity problem formulation without explicitly considering atmospheric turbulence. We will then, for the purposes of design, represent gusts as a perturbation in the velocity states of the helicopter model and include this disturbance as an extra input to the S/KS design problem. The resulting controller is seen to be substantially better at rejecting atmospheric turbulence than the earlier standard S/KS design.

12.2.2 The helicopter model

The aircraft model used in our work is representative of the Westland Lynx, a twin-engined multi-purpose military helicopter, approximately 9000 lbs gross weight, with a four-blade semi-rigid main rotor. The unaugmented aircraft is unstable, and exhibits many of the cross-couplings characteristic of a single main-rotor helicopter. In addition to the basic rigid body, engine and actuator components, the model also includes second order rotor flapping and coning modes for off-line use. The model has the advantage that essentially the same code can be used for a real-time piloted simulation as for a workstation-based off-line handling qualities assessment.

The equations governing the motion of the helicopter are complex and difficult

to formulate with high levels of precision. For example, the rotor dynamics are particularly difficult to model. A robust design methodology is therefore essential for high performance helicopter control. The starting point for this study was to obtain

State	Description
θ	Pitch attitude
ϕ	Roll attitude
p	Roll rate (body-axis)
q	Pitch rate (body-axis)
ξ	Yaw rate
v_x	Forward velocity
v_y	Lateral velocity
v_z	Vertical velocity

Table 12.1: Helicopter state vector

an eighth-order differential equation modelling the small-perturbation rigid motion of the aircraft about hover. The corresponding state-space model is

$$\dot{x} = Ax + Bu \tag{12.1}$$
$$y = Cx \tag{12.2}$$

where the matrices A, B and C for the appropriately scaled system are available over the Internet as described in the preface. The 8 state rigid body vector x is given in the Table 12.1. The outputs consist of four controlled outputs

- Heave velocity $\dot{H}$
- Pitch attitude θ
- Roll attitude ϕ
- Heading rate $\dot{\psi}$

$\Big\}\ y_1$

together with two additional (body-axis) measurements

- Roll rate p
- Pitch rate q

$\Big\}\ y_2$

The controller (or pilot in manual control) generates four blade angle demands which are effectively the helicopter inputs, since the actuators (which are typically modelled as first order lags) are modelled as unity gains in this study. The blade angles are

- main rotor collective
- longitudinal cyclic
- lateral cyclic
- tail rotor collective

$\Big\}\ u$

The action of each of these blade angles can be briefly described as follows. The main rotor collective changes all the blades of the main rotor by an equal amount and so

roughly speaking controls lift. The longitudinal and lateral cyclic inputs change the main rotor blade angles differently thereby tilting the lift vector to give longitudinal and lateral motion, respectively. The tail rotor is used to balance the torque generated by the main rotor, and so stops the helicopter spinning around; it is also used to give lateral motion. This description, which assumes the helicopter inputs and outputs are decoupled, is useful to get a feeling of how a helicopter works but the dynamics are actually highly coupled. They are also unstable, and about some operating points exhibit non-minimum phase characteristics.

We are interested in the design of *full-authority controllers*, which means that the controller has total control over the blade angles of the main and tail rotors, and is interposed between the pilot and the actuation system. It is normal in conventional helicopters for the controller to have only limited authority leaving the pilot to close the loop for much of the time (manual control). With a full-authority controller, the pilot merely provides the reference commands.

One degree-of-freedom controllers as shown in Figure 12.1 are to be designed. Notice that in the standard one degree-of-freedom configuration the pilot reference

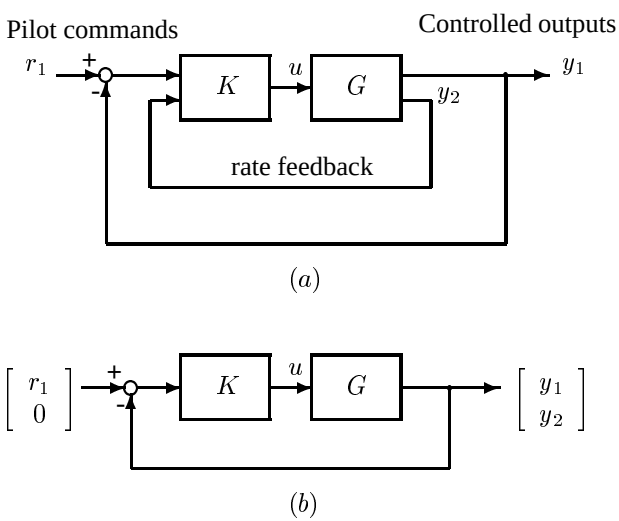

Figure 12.1: Helicopter control structure (a) as implemented, (b) in the standard one degree-of-freedom configuration

commands r_1 are augmented by a zero vector because of the rate feedback signals. These zeros indicate that there are no *a priori* performance specifications on $y_2 = [p \quad q]^T$.

12.2.3 $\mathcal{H}_\infty$ mixed-sensitivity design

We will consider the $\mathcal{H}_\infty$ mixed-sensitivity design problem illustrated in Figure 12.2. It can be viewed as a tracking problem as previously discussed in Chapter 9 (see

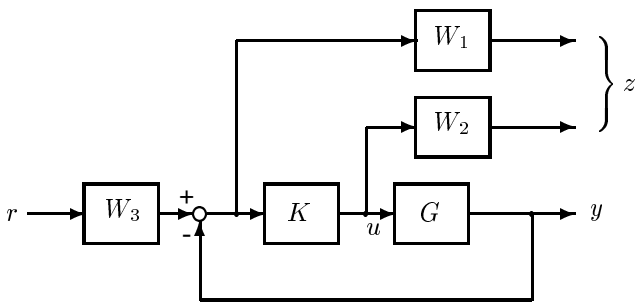

Figure 12.2: S/KS mixed-sensitivity minimization

Figure 9.11), but with an additional weight W_3. W_1 and W_2 are selected as loop-shaping weights whereas W_3 is signal-based. The optimization problem is to find a stabilizing controller K to minimize the cost function

$$\left\| \begin{bmatrix} W_1 S W_3 \\ W_2 K S W_3 \end{bmatrix} \right\|_\infty \tag{12.3}$$

This cost was also considered by Yue and Postlethwaite (1990) in the context of helicopter control. Their controller was successfully tested on a piloted flight simulator at DRA Bedford and so we propose to use the same weights here. The design weights W_1, W_2 and W_3 were selected as

$$\begin{aligned} W_1 &= diag\left\{ 0.5\frac{s+12}{s+0.012},\ 0.89\frac{s+2.81}{s+0.005},\ 0.89\frac{s+2.81}{s+0.005}, \right. \\ &\qquad \left. 0.5\frac{s+10}{s+0.01},\ \frac{2s}{(s+4)(s+4.5)},\ \frac{2s}{(s+4)(s+4.5)} \right\} \qquad (12.4) \\ W_2 &= 0.5\frac{s+0.0001}{s+10} I_4 \qquad (12.5) \\ W_3 &= diag\{1,\ 1,\ 1,\ 1,\ 0.1,\ 0.1\} \qquad (12.6) \end{aligned}$$

The reasoning behind these selections of Yue and Postlethwaite (1990) is summarized below.

Selection of $W_1(s)$: For good tracking accuracy in each of the controlled outputs the sensitivity function is required to be small. This suggests forcing integral action into the controller by selecting an s^{-1} shape in the weights associated with the controlled outputs. It was not thought necessary to have exactly zero steady-state

errors and therefore these weights were given a finite gain of 500 at low frequencies. (Notice that a pure integrator cannot be included in W_1 anyway, since the standard $\mathcal{H}_\infty$ optimal control problem would not then be well posed in the sense that the corresponding generalized plant P could not then be stabilized by the feedback controller K). In tuning W_1 it was found that a finite attenuation at high frequencies was useful in reducing overshoot. Therefore, high-gain low-pass filters were used in the primary channels to give accurate tracking up to about 6 rad/s. The presence of unmodelled rotor dynamics around 10 rad/s limits the bandwidth of W_1. With four inputs to the helicopter, we can only expect to independently control four outputs. Because of the rate feedback measurements the sensitivity function S is a six by six matrix and therefore two of its singular values (corresponding to p and q) are always close to one across all frequencies. All that can be done in these channels is to improve the disturbance rejection properties around crossover, 4 to 7 rad/s, and this was achieved using second-order band-pass filters in the rate channels of W_1.

Selection of $W_2(s)$: The same first-order high-pass filter is used in each channel with a corner frequency of 10 rad/s to limit input magnitudes at high frequencies and thereby limit the closed-loop bandwidth. The high frequency gain of W_2 can be increased to limit fast actuator movement. The low frequency gain of W_2 was set to approximately -100 dB to ensure that the cost function is dominated by W_1 at low frequencies.

Selection of $W_3(s)$: W_3 is a weighting on the reference input r. It is chosen to be a constant matrix with unity weighting on each of the output commands and a weighting of 0.1 on the fictitious rate demands. The reduced weighting on the rates (which are not directly controlled) enables some disturbance rejection on these outputs, without them significantly affecting the cost function. The main aim of W_3 is to force equally good tracking of each of the primary signals.

For the controller designed using the above weights, the singular value plots of S and KS are shown in Figures 12.3(a) and 12.3(b). These have the general shapes and bandwidths designed for and, as already mentioned, the controlled system performed well in piloted simulation. The effects of atmospheric turbulence will be illustrated later after designing a second controller in which disturbance rejection is explicitly included in the design problem.

12.2.4 Disturbance rejection design

In the design below we will assume that the atmospheric turbulence can be modelled as gust velocity components that perturb the helicopter's velocity states v_x, v_y and v_z by $d = [\,d_1 \quad d_2 \quad d_3\,]^T$ as in the following equations. The disturbed system is therefore expressed as

$$\dot{x} \quad = \quad Ax + A \begin{bmatrix} 0 \\ d \end{bmatrix} + Bu \tag{12.7}$$

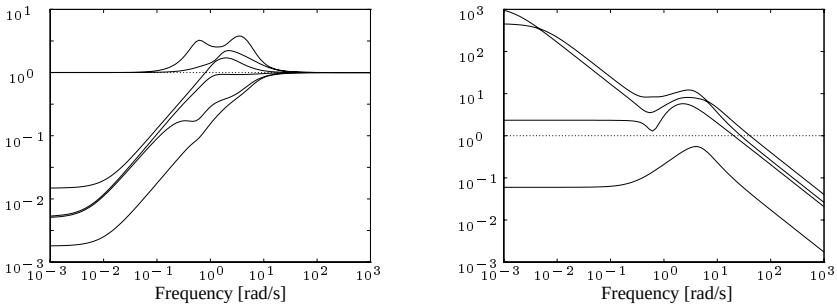

(a) S (b) KS

Figure 12.3: Singular values of S and KS (S/KS design)

$$y = Cx. \tag{12.8}$$

Define $B_d \stackrel{\triangle}{=}$ columns 6,7 and 8 of A. Then we have

$$\dot{x} = Ax + Bu + B_d d \tag{12.9}$$
$$y = Cx \tag{12.10}$$

which in transfer function terms can be expressed as

$$y = G(s)u + G_d(s)d \tag{12.11}$$

where $G(s) = C(sI - A)^{-1}B$, and $G_d(s) = C(sI - A)^{-1}B_d$. The design problem we will solve is illustrated in Figure 12.4. The optimization problem is to find a stabilizing controller K that minimizes the cost function

$$\left\| \begin{bmatrix} W_1 S W_3 & -W_1 S G_d W_4 \\ W_2 K S W_3 & -W_2 K S G_d W_4 \end{bmatrix} \right\|_\infty \tag{12.12}$$

which is the $\mathcal{H}_\infty$ norm of the transfer function from $\begin{bmatrix} r \\ d \end{bmatrix}$ to z. This is easily cast into the general control configuration and solved using standard software. Notice that if we set W_4 to zero the problem reverts to the S/KS mixed-sensitivity design of the previous subsection. To synthesize the controller we used the same weights W_1, W_2 and W_3 as in the S/KS design, and selected $W_4 = \alpha I$, with α a scalar parameter used to emphasize disturbance rejection. After a few iterations we finalized on $\alpha = 30$. For this value of α, the singular value plots of S and KS, see Figures 12.5(a) and 12.5(b), are quite similar to those of the S/KS design, but as we will see in the next subsection there is a significant improvement in the rejection of gusts. Also, since G_d shares the same dynamics as G, and W_4 is a constant matrix, the degree of the disturbance rejection controller is the same as that for the S/KS design.

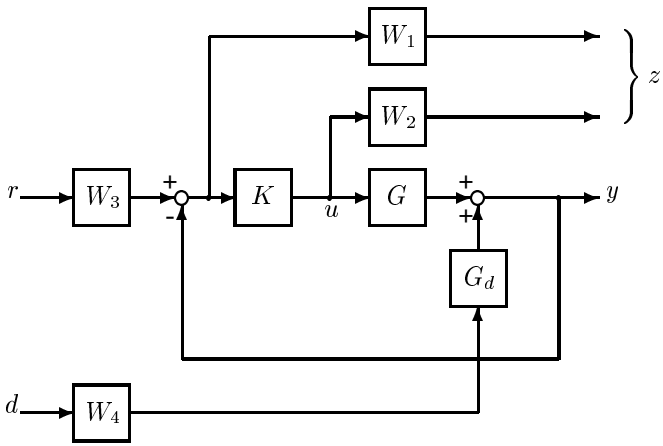

Figure 12.4: Disturbance rejection design

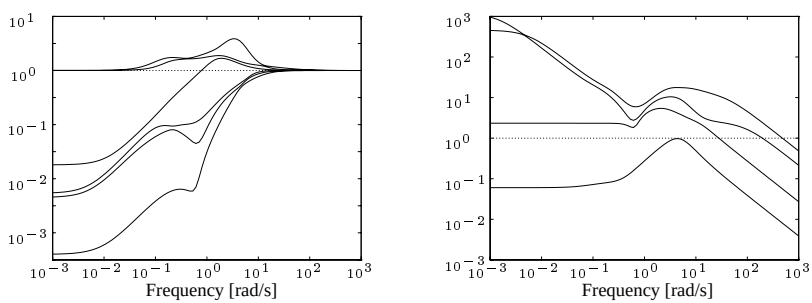

(a) S (b) KS

Figure 12.5: Singular values of S and KS (disturbance rejection design)

12.2.5 Comparison of disturbance rejection properties of the two designs

To compare the disturbance rejection properties of the two designs we simulated both controllers on the RHM nonlinear helicopter model equipped with a statistical discrete gust model for atmospheric turbulence, (Dahl and Faulkner, 1979). With this simulation facility, gusts cannot be generated at hover and so the nonlinear model was trimmed at a forward flight speed of 20 knots (at an altitude of 100 ft), and the effect of turbulence on the four controlled outputs observed. Recall that both designs were based on a linearized model about hover and therefore these tests at 20 knots also

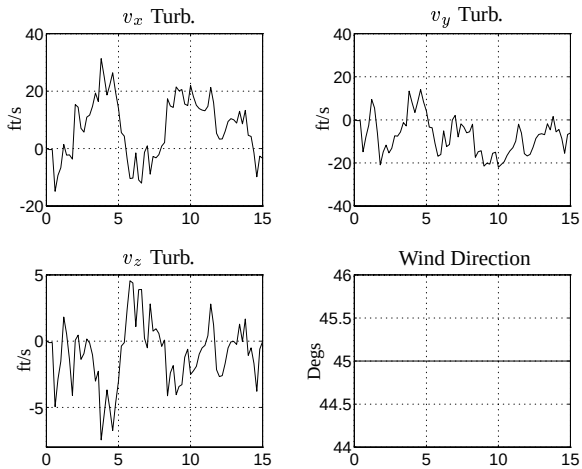

Figure 12.6: Velocity components of turbulence (time in seconds)

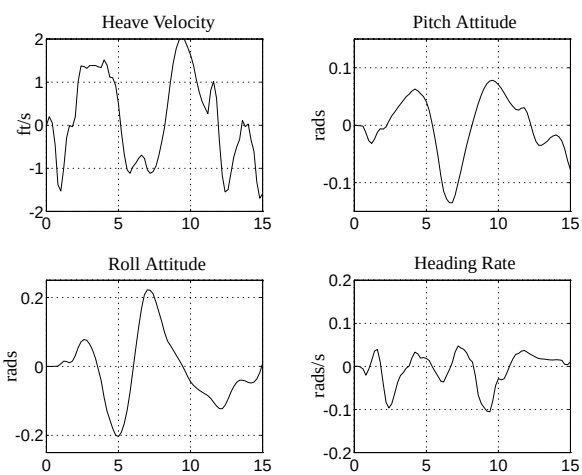

Figure 12.7: Response to turbulence of the S/KS design (time in seconds)

demonstrate the robustness of the controllers. Tests were carried out for a variety of gusts, and in all cases the disturbance rejection design was significantly better than the S/KS design.

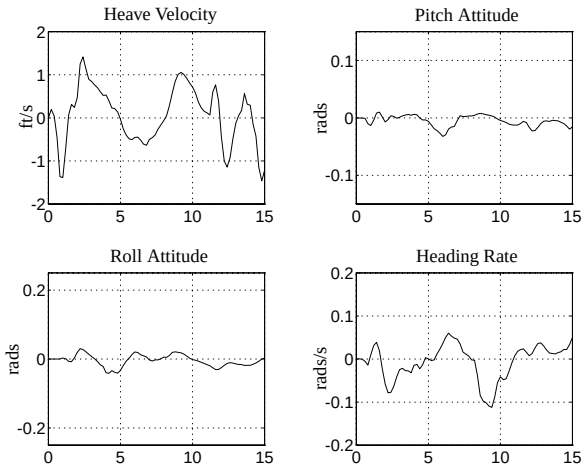

Figure 12.8: Response to turbulence of the disturbance rejection design (time in seconds)

In Figure 12.6, we show a typical gust generated by the RHM. The effects of this on the controlled outputs are shown in Figures 12.7 and 12.8 for the S/KS design and the disturbance rejection design, respectively. Compared with the S/KS design, the disturbance rejection controller practically halves the turbulence effect on heavy velocity, pitch attitude and roll attitude. The change in the effect on heading rate is small.

12.2.6 Conclusions

The two controllers designed were of the same degree and had similar frequency domain properties. But by incorporating knowledge about turbulence activity into the second design, substantial improvements in disturbance rejection were achieved. The reduction of the turbulence effects by a half in heave velocity, pitch attitude and roll attitude indicates the possibility of a significant reduction in a pilot's workload, allowing more aggressive manoeuvers to be carried out with greater precision. Passenger comfort and safety would also be increased.

The study was primarily meant to illustrate the ease with which information about disturbances can be beneficially included in controller design. The case study also demonstrated the selection of weights in $\mathcal{H}_\infty$ mixed-sensitivity design. To read how the $\mathcal{H}_\infty$ methods have been successfully used and tested in flight on a Bell 205 fly-by-wire helipcopter, see Postlethwaite et al. (1999) and Smerlas et al. (2001).

12.3 Aero-engine control

In this case study, we apply a variety of tools to the problem of output selection, and illustrate the application of the two degrees-of-freedom $\mathcal{H}_\infty$ loop-shaping design procedure.

12.3.1 Problem description

This case study explores the application of advanced control techniques to the problem of control structure design and robust multivariable controller design for a high performance gas turbine engine. The engine under consideration is the Spey engine which is a Rolls-Royce 2-spool reheated turbofan, used to power modern military aircraft. The engine has two compressors: a low pressure (LP) compressor or fan, and a high pressure (HP) or core compressor as shown in Figure 12.9. The

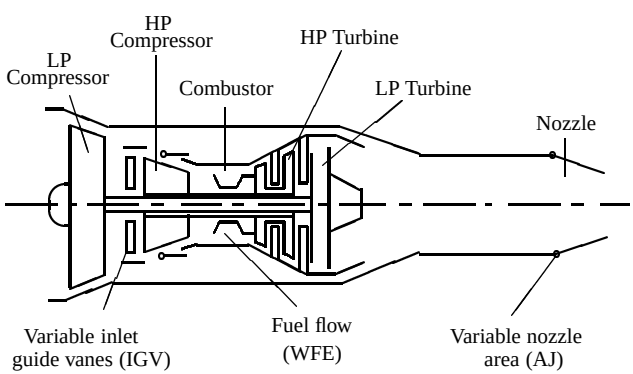

Figure 12.9: Schematic of the aero-engine

high pressure flow at the exit of the core compressor is combusted and allowed to partially expand through the HP and LP turbines which drive the two compressors. The flow finally expands to atmospheric pressure at the nozzle exit, thus producing thrust for aircraft propulsion. The efficiency of the engine and the thrust produced depends on the pressure ratios generated by the two compressors. If the pressure ratio across a compressor exceeds a certain maximum, it may no longer be able to hold the pressure head generated and the flow will tend to reverse its direction. This happens in practice, with the flow actually going negative, but it is only a momentary effect. When the back pressure has cleared itself, positive flow is re-established but, if flow conditions do not change, the pressure builds up causing flow reversal again. Thus the flow surges back and forth at high frequency, the phenomenon being referred to as *surge*. Surging causes excessive aerodynamic pulsations which are transmitted

through the whole machine and must be avoided at all costs. However, for higher performance and greater efficiency the compressors must also be operated close to their surge lines. The primary aim of the control system is thus to control engine thrust whilst regulating compressor surge margins. But these engine parameters, namely thrust and the two compressor surge margins, are not directly measurable. There are, however, a number of measurements available which represent these quantities, and our first task is to choose from the available measurements, the ones that are in some sense better for control purposes. This is the problem of output selection as discussed in Chapter 10.

The next step is the design of a robust multivariable controller which provides satisfactory performance over the entire operating range of the engine. Since the aero-engine is a highly nonlinear system, it is normal for several controllers to be designed at different operating points and then to be scheduled across the flight envelope. Also in an aero-engine there are a number of parameters, apart from the ones being primarily controlled, that are to be kept within specified safety limits, e.g. the turbine blade temperature. The number of parameters to be controlled and/or limited exceeds the number of available inputs, and hence all these parameters cannot be controlled independently at the same time. The problem can be tackled by designing a number of scheduled controllers, each for a different set of output variables, which are then switched between, depending on the most significant limit at any given time. The switching is usually done by means of lowest-wins or highest-wins gates, which serve to propagate the output of the most suitable controller to the plant input. Thus, a switched gain-scheduled controller can be designed to cover the full operating range and all possible configurations. In Postlethwaite et al. (1995) a digital multi-mode scheduled controller is designed for the Spey engine under consideration here. In their study gain-scheduling was not required to meet the design specifications. Below we will describe the design of a robust controller for the primary engine outputs using the two degrees-of-freedom $\mathcal{H}_\infty$ loop-shaping approach. The same methodology was used in the design of Postlethwaite et al. (1995) which was successfully implemented and tested on the Spey engine.

12.3.2 Control structure design: output selection

The Spey engine has three inputs, namely fuel flow (WFE), a nozzle with a variable area (AJ), and inlet guide vanes with a variable angle setting (IGV):

$$u = [\,\mathrm{WFE} \quad \mathrm{AJ} \quad \mathrm{IGV}\,]^T$$

In this study, there are six output measurements available,

$$y_{\mathrm{all}} = [\,\mathrm{NL} \quad \mathrm{OPR1} \quad \mathrm{OPR2} \quad \mathrm{LPPR} \quad \mathrm{LPEMN} \quad \mathrm{NH}\,]^T$$

as described below. For each one of the six output measurements, a look-up table provides its desired optimal value (set point) as a function of the operating point.

However, with three inputs we can only control three outputs independently so the first question we face is, which three?

Engine thrust (one of the parameters to be controlled) can be defined in terms of the LP compressor's spool speed (NL), the ratio of the HP compressor's outlet pressure to engine inlet pressure (OPR1), or the engine overall pressure ratio (OPR2). We will choose from these three measurements the one that is best for control.

- Engine thrust: Select one of NL, OPR1 and OPR2 (outputs 1, 2 and 3).

Similarly, surge margin of the LP compressor can be represented by either the LP compressor's pressure ratio (LPPR) or the LP compressor's exit Mach number measurement (LPEMN), and a selection between the two has to be made.

- Surge margin: Select one of LPPR and LPEMN (outputs 4 and 5).

In this study we will not consider control of the HP compressor's surge margin, or other configurations concerned with the limiting of engine temperatures. Our third output will be the HP compressor's spool speed (NH), which it is also important to maintain within safe limits. (NH is actually the HP spool speed made dimensionless by dividing by the square root of the total inlet temperature and scaled so that it is a percentage of the maximum spool speed at a standard temperature of $288.15\,^{\circ}$K).

- Spool speed: Select NH (output 6).

We have now subdivided the available outputs into three subsets, and decided to select one output from each subset. This gives rise to the six candidate output sets as listed in Table 12.2.

We now apply some of the tools given in Chapter 10 for tackling the output selection problem. It is emphasized at this point that a good physical understanding of the plant is very important in the context of this problem, and some measurements may have to be screened beforehand on practical grounds. A 15 state linear model of the engine (derived from a nonlinear simulation at 87% of maximum thrust) will be used in the analysis that follows. The model is available over the Internet (as described in the preface), along with actuator dynamics which result in a plant model of 18 states for controller design. The nonlinear model used in this case study was provided by the UK Defence Research Agency at Pyestock with the permission of Rolls-Royce Military Aero Engines Ltd.

Scaling. Some of the tools we will use for control structure selection are dependent on the scalings employed. Scaling the inputs and the candidate measurements therefore, is vital before comparisons are made and can also improve the conditioning of the problem for design purposes. We use the method of scaling described in Section 9.4.2. The outputs are scaled such that equal magnitudes of cross-coupling into each of the outputs are equally undesirable. We have chosen to scale the thrust-related outputs such that one unit of each scaled measurement

represents 7.5% of maximum thrust. A step demand on each of these scaled outputs would thus correspond to a demand of 7.5% (of maximum) in thrust. The surge margin-related outputs are scaled so that one unit corresponds to 5% surge margin. If the controller designed provides an interaction of less than 10% between the scaled outputs (for unit reference steps), then we would have 0.75% or less change in thrust for a step demand of 5% in surge margin, and a 0.5% or less change in surge margin for a 7.5% step demand in thrust. The final output NH (which is already a scaled variable) was further scaled (divided by 2.2) so that a unit change in NH corresponds to a 2.2% change in NH. The inputs are scaled by 10% of their expected ranges of operation.

Set No.	Candidate controlled outputs	RHP zeros < 100 rad/sec	$\underline{\sigma}\,(G(0))$
1	NL, LPPR, NH (1, 4, 6)	none	0.060
2	OPR1, LPPR, NH (2, 4, 6)	none	0.049
3	OPR2, LPPR, NH (3, 4, 6)	30.9	0.056
4	NL, LPEMN, NH (1, 5, 6)	none	0.366
5	OPR1, LPEMN, NH (2, 5, 6)	none	0.409
6	OPR2, LPEMN, NH (3, 5, 6)	27.7	0.392

Table 12.2: RHP zeros and minimum singular value for the six candidate output sets

Steady-state model. With these scalings the steady-state model $y_{\text{all}} = G_{\text{all}}u$ (with all the candidate outputs included) and the corresponding RGA-matrix, $\Lambda = G_{\text{all}} \times G_{\text{all}}^{\dagger^T}$, are given by

$$G_{\text{all}} = \begin{bmatrix} 0.696 & -0.046 & -0.001 \\ 1.076 & -0.027 & 0.004 \\ 1.385 & 0.087 & -0.002 \\ 11.036 & 0.238 & -0.017 \\ -0.064 & -0.412 & 0.000 \\ 1.474 & -0.093 & 0.983 \end{bmatrix} \quad \Lambda(G_{\text{all}}) = \begin{bmatrix} 0.009 & 0.016 & 0.000 \\ 0.016 & 0.008 & -0.000 \\ 0.006 & 0.028 & -0.000 \\ 0.971 & -0.001 & 0.002 \\ -0.003 & 0.950 & 0.000 \\ 0.002 & -0.000 & 0.998 \end{bmatrix} \tag{12.13}$$

and the singular value decomposition of $G_{\text{all}}(0) = U_0\Sigma_0 V_0^H$ is

$$U_0 = \begin{bmatrix} 0.062 & 0.001 & -0.144 & -0.944 & -0.117 & -0.266 \\ 0.095 & 0.001 & -0.118 & -0.070 & -0.734 & 0.659 \\ 0.123 & -0.025 & 0.133 & -0.286 & 0.640 & 0.689 \\ 0.977 & -0.129 & -0.011 & 0.103 & -0.001 & -0.133 \\ -0.006 & 0.065 & -0.971 & 0.108 & 0.195 & 0.055 \\ 0.131 & 0.989 & 0.066 & -0.000 & 0.004 & -0.004 \end{bmatrix}$$

$$\Sigma_0 = \begin{bmatrix} 11.296 & 0 & 0 \\ 0 & 0.986 & 0 \\ 0 & 0 & 0.417 \\ 0 & 0 & 0 \\ 0 & 0 & 0 \\ 0 & 0 & 0 \end{bmatrix} \quad V_0 = \begin{bmatrix} 1.000 & -0.007 & -0.021 \\ 0.020 & -0.154 & 0.988 \\ 0.010 & 0.988 & 0.154 \end{bmatrix}$$

The RGA-matrix of G_{all}, the overall non-square gain matrix, is sometimes a useful screening tool when there are many alternatives. The six row-sums of the RGA-matrix are

$$\Lambda_\Sigma = [\,0.025 \quad 0.023 \quad 0.034 \quad 0.972 \quad 0.947 \quad 1.000\,]^T$$

and from (10.12) this indicates that we should select outputs 4, 5 and 6 (corresponding to the three largest elements) in order to maximize the projection of the selected outputs onto the space corresponding to the three non-zero singular values. However, this selection is not one of our six candidate output sets because there is no output directly related to engine thrust (outputs 1, 2 and 3).

We now proceed with a more detailed input-output controllability analysis of the six candidate output sets. In the following, $G(s)$ refers to the transfer function matrix for the effect of the three inputs on the selected three outputs.

Minimum singular value. In Chapter 10, we showed that a reasonable criterion for selecting controlled outputs y is to make $\|G^{-1}(y - y_{opt})\|$ small, in particular at steady-state. Here $y - y_{opt}$ is the deviation in y from its optimal value. At steady-state this deviation arises mainly from errors in the (look-up table) set point due to disturbances and unknown variations in the operating point. If we assume that, with the scalings given above, the magnitude $|(y - y_{opt})_i|$ is similar (close to 1) for each of the six outputs, then we should select a set of outputs such that the elements in $G^{-1}(0)$ are small, or alternatively, such that $\underline{\sigma}(G(0))$ is as large as possible. In Table 12.2 we have listed $\underline{\sigma}(G(0))$ for the six candidate output sets. We conclude that we can eliminate sets 1, 2 and 3, and consider only sets 4, 5 and 6. For these three sets we find that the value of $\bar{\sigma}(G(0))$ is between 0.366 and 0.409 which is only slightly smaller than $\bar{\sigma}(G_{\text{all}}(0)) = 0.417$.

Remark. The three eliminated sets all include output 4, LPPR. Interestingly, this output is associated with the largest element in the gain matrix $G_{\text{all}}(0)$ of 11.0, and is thus also associated with the largest singular value (as seen from the first column of U). This illustrates that the preferred choice is often not associated with $\bar{\sigma}(G)$.

Right-half plane zeros. Right-half plane (RHP) zeros limit the achievable performance of a feedback loop by limiting the open-loop gain-bandwidth product. They can be a cause of concern, particularly if they lie within the desired closed-loop bandwidth. Also, choosing different outputs for feedback control can give rise to different numbers of RHP zeros at different locations. The choice of outputs should be such that a minimum number of RHP zeros are encountered, and should be as far removed from the imaginary axis as possible.

Table 12.2 shows the RHP zeros slower than 100 rad/sec for all combinations of prospective output variables. The closed-loop bandwidth requirement for the aero-engine is approximately 10 rad/sec. RHP zeros close to this value or smaller (closer to the origin) will therefore, cause problems and should be avoided. It can be seen that the variable OPR2 introduces (relatively) slow RHP zeros. It was observed that these zeros move closer to the origin at higher thrust levels. Thus Sets 3 and 6 are unfavourable for closed-loop control. This along with the minimum singular value analysis leaves us with sets 4 and 5 for further consideration

Relative gain array (RGA). We here consider the RGAs of the candidate square transfer function matrices $G(s)$ with three outputs,

$$\Lambda(G(s)) = G(s) \times G^{-T}(s) \tag{12.14}$$

In Section 3.6.2, it is argued that the RGA provides useful information for the analysis of input-output controllability and for the pairing of inputs and outputs. Specifically input and output variables should be paired so that the diagonal elements of the RGA are as close as possible to unity. Furthermore, if the plant has large RGA elements and an inverting controller is used, the closed-loop system will have little robustness in the face of diagonal input uncertainty. Such a perturbation is quite common due to uncertainty in the actuators. Thus we want Λ to have small elements and for diagonal dominance we want $\Lambda - I$ to be small. These two objectives can be combined in the single objective of a small RGA-number, defined as

$$\text{RGA-number} \triangleq \|\Lambda - I\|_{\text{sum}} = \sum_{i=j} \mid 1 - \lambda_{ij} \mid + \sum_{i \neq j} \mid \lambda_{ij} \mid \tag{12.15}$$

The lower the RGA number, the more preferred is the control structure. Before calculating the RGA number over frequency we rearranged the output variables so that the steady-state RGA matrix was as close as possible to the identity matrix.

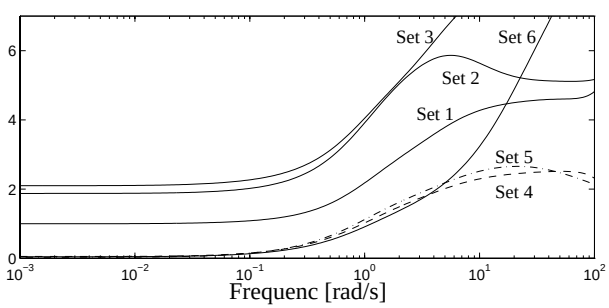

Figure 12.10: RGA numbers

The RGA numbers for the six candidate output sets are shown in Figure 12.10. As in the minimum singular value analysis above, we again see that Sets 1,2 and 3 are less

favourable. Once more, sets 4 and 5 are the best but too similar to allow a decisive selection.

Hankel singular values. Notice that Sets 4 and 5 differ only in one output variable, NL in Set 4 and OPR1 in Set 5. Therefore, to select between them we next consider the Hankel singular values of the two transfer functions between the three inputs and output NL and output OPR1, respectively. Hankel singular values reflect the joint controllability and observability of the states of a balanced realization (as described in Section 11.3). Recall that the Hankel singular values are invariant under state transformations but they do depend on scaling.

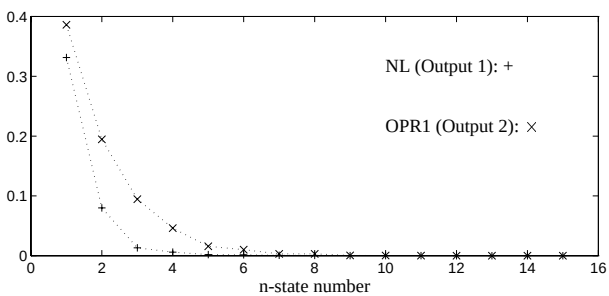

Figure 12.11: Hankel singular values

Figure 12.11 shows the Hankel singular values of the two transfer functions for outputs NL and OPR1, respectively. The Hankel singular values for OPR1 are larger, which indicates that OPR1 has better state controllability and observability properties than NL. In other words, output OPR1 contains more information about the system internal states than output NL. It therefore seems to be preferable to use OPR1 for control purposes rather than NL, and hence (in the absence of no other information) Set 5 is our final choice.

12.3.3 A two degrees-of-freedom $\mathcal{H}_\infty$ loop-shaping design

The design procedure given in Section 9.4.3 will be used to design a two degrees-of-freedom $\mathcal{H}_\infty$ loop-shaping controller for the 3-input 3-output plant G. An 18 state linear plant model G (including actuator dynamics), is available over the Internet. It is based on scaling, output selection, and input-output pairing as described below. To summarize, the selected outputs (Set 5) are

- engine inlet pressure, OPR1
- LP compressor's exit mach number measurement, LPEMN
- HP compressor's spool speed, NH

and the corresponding inputs are

- fuel flow, WFE
- nozzle area, AJ
- inlet guide vane angle, IGV

The corresponding steady-state ($s = 0$) model and RGA-matrix is

$$G = \begin{bmatrix} 1.076 & -0.027 & 0.004 \\ -0.064 & -0.412 & 0.000 \\ 1.474 & -0.093 & 0.983 \end{bmatrix}, \quad \Lambda(G) = \begin{bmatrix} 1.002 & 0.004 & -0.006 \\ 0.004 & 0.996 & -0.000 \\ -0.006 & -0.000 & 1.006 \end{bmatrix} \tag{12.16}$$

Pairing of inputs and outputs. The pairing of inputs and outputs is important because it makes the design of the prefilter easier in a two degrees-of-freedom control configuration and simplifies the selection of weights. It is of even greater importance if a decentralized control scheme is to be used, and gives insight into the working of the plant. In Chapter 10, it is argued that negative entries on the principal diagonal of the steady-state RGA should be avoided and that the outputs in G should be (re)arranged such that the RGA is close to the identity matrix. For the selected output set, we see from (12.16) that no rearranging of the outputs is needed. That is, we should pair OPR1, LPEMN and NH with WFE, AJ and IGV, respectively.

$\mathcal{H}_\infty$ **loop-shaping design.** We follow the design procedure given in Section 9.4.3. In steps 1 to 3 we discuss how pre- and post-compensators are selected to obtain the desired shaped plant (loop shape) $G_s = W_2 G W_1$ where $W_1 = W_p W_a W_b$. In steps 4 to 6 we present the subsequent $\mathcal{H}_\infty$ design.

1. The singular values of the plant are shown in Figure 12.12(a) and indicate a need for extra low frequency gain to give good steady-state tracking and disturbance rejection. The precompensator weight is chosen as simple integrators, i.e. $W_p = \frac{1}{s} I_3$, and the post-compensator weight is selected as $W_2 = I_3$.
2. $W_2 G W_p$ is next aligned at 7 rad/sec. The align gain W_a (used in front of W_p) is the approximate real inverse of the shaped system at the specified frequency. The

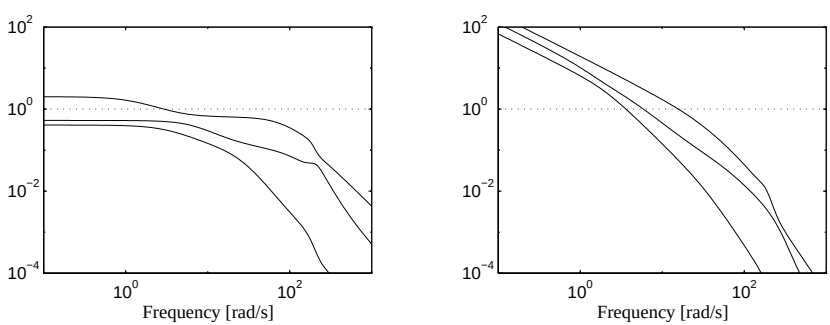

(a) Plant (b) Shaped plant

Figure 12.12: Singular values for plant and shaped plant

crossover is thus adjusted to 7 rad/sec in order to give a closed-loop bandwidth of approximately 10 rad/sec. Alignment should not be used if the plant is ill-conditioned with large RGA elements at the selected alignment frequency. In our case the RGA elements are small (see Figure 12.10) and hence alignment is not expected to cause problems.

3. An additional gain W_g is used in front of the align gain to give some control over actuator usage. W_g is adjusted so that the actuator rate limits are not exceeded for reference and disturbance steps on the scaled outputs. By some trial and error, W_g is chosen to be $\mathrm{diag}(1, 2.5, 0.3)$. This indicates that the second actuator (AJ) is made to respond at higher rates whereas the third actuator (IGV) is made slower. The shaped plant now becomes $G_s = GW_1$ where $W_1 = W_p W_a W_g$. Its singular values are shown in Figure 12.12(b).
4. γ_{min} in (9.66) for this shaped plant is found to be 2.3 which indicates that the shaped plant is compatible with robust stability.
5. ρ is set to 1 and the reference model T_{ref} is chosen as $T_{\mathrm{ref}} = \mathrm{diag}\{\frac{1}{0.018s+1}, \frac{1}{0.008s+1}, \frac{1}{0.2s+1}\}$. The third output NH is thus made slower than the other two in following reference inputs.
6. The standard $\mathcal{H}_\infty$ optimization defined by P in (9.87) is solved. γ iterations are performed and a slightly suboptimal controller achieving $\gamma = 2.9$ is obtained. Moving closer to optimality introduces very fast poles in the controller which, if the controller is to be discretized, would ask for a very high sample rate. Choosing a slightly suboptimal controller alleviates this problem and also improves on the H_2 performance. The prefilter is finally scaled to achieve perfect steady-state model matching. The controller (with the weights W_1 and W_2) has 27 states.

12.3.4 Analysis and simulation results

Step responses of the linear controlled plant model are shown in Figure 12.13. The decoupling is good with less than 10% interactions. Although not shown here

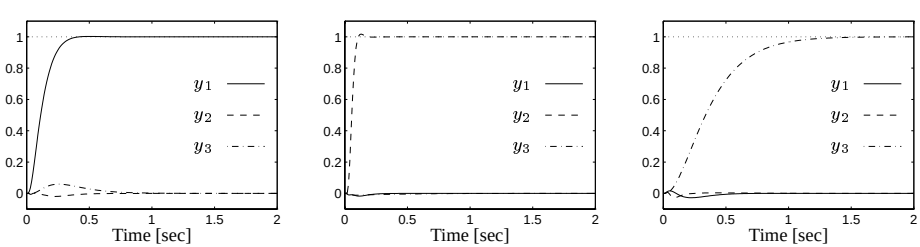

(a) Step in r_1 (b) Step in r_2 (c) Step in r_3

Figure 12.13: Reference step responses

the control inputs were analyzed and the actuator signals were found to lie within specified limits. Responses to disturbance steps on the outputs were also seen to meet the problem specifications. Notice that because there are two degrees-of-freedom in the controller structure, the reference to output and disturbance to output transfer functions can be given different bandwidths.

The robustness properties of the closed-loop system are now analyzed. Figure 12.14(a) shows the singular values of the sensitivity function. The peak value

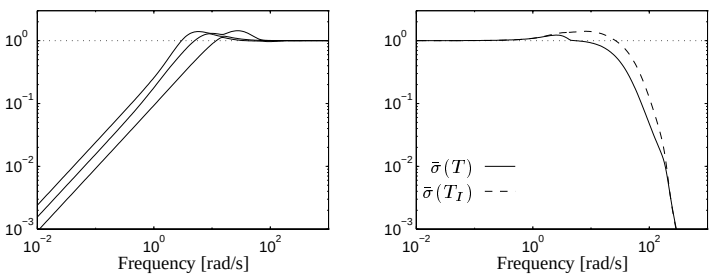

(a) Singular values, $\bar{\sigma}_i(S)$ (b) $\bar{\sigma}(T)$ and $\bar{\sigma}(T_I)$

Figure 12.14: Sensitivity and complementary sensitivity functions

is less than 2 (actually it is $1.44 = 3.2$ dB), which is considered satisfactory. Figure 12.14(b) shows the maximum singular values of $T = (I - GW_1K_2)^{-1}GW_1K_2$ and $T_I = (I - W_1K_2G)^{-1}W_1K_2G$. Both of these have small peaks and go to zero quickly at high frequencies. From Section 9.2.2, this indicates good robustness both with respect to multiplicative output and multiplicative input plant perturbations.

Nonlinear simulation results are shown in Figure 12.15. Reference signals are given

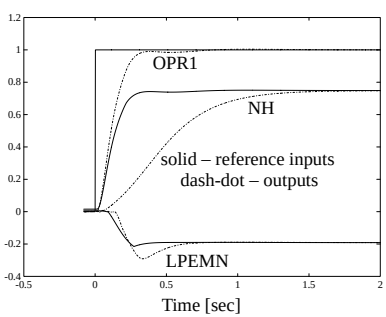

Figure 12.15: Nonlinear simulation results

to each of the scaled outputs simultaneously. The solid lines show the references,

and the dash-dot lines, the outputs. It can be seen that the controller exhibits good performance with low interactions.

12.3.5 Conclusions

The case study has demonstrated the ease with which the two degrees-of-freedom $\mathcal{H}_\infty$ loop-shaping design procedure can be applied to a complex engineering system. Some tools for control structure design have also been usefully applied to the aero-engine example. We stress that a good control structure selection is very important. It results in simpler controllers and in general, a simpler design exercise.

12.4 Distillation process

A typical distillation column is shown in Figure 10.8 on page 434. The overall 5×5 control problem is discussed in Example 10.5 (page 433) and you are advised to read this first. The commonly used LV- and DV-configurations, which are discussed below, are partially controlled systems where 3 loops for liquid level and pressure have already been closed.

For a general discussion on distillation column control, the reader is also referred to Shinskey (1984), Skogestad and Morari (1987a) and the survey paper by Skogestad (1997).

We have throughout the book studied a particular high-purity binary distillation column with 40 theoretical stages (39 trays and a reboiler) plus a total condenser. This is "column A" in Skogestad et al. (1990). The feed is an equimolar liquid mixture of two components with a relative volatility of 1.5. The pressure p is assumed constant (perfect control of p using V_T as an input). The operating variables (e.g. reflux and boilup rates) are such that we nominally have 99% purity for each product (y_D and x_B). The nominal holdups on all stages, including the reboiler and condenser, are $M_i^*/F = 0.5$ min. The liquid flow dynamics are modelled by a simple linear relationship, $L_i(t) = L_i^* + (M_i(t) - M_i^*)/\tau_L$, where $\tau_L = 0.063$ min (the same value is used on all trays). No actuator or measurement dynamics are included. This results in a model with 82 states. This distillation process is difficult to control because of strong interactions between the two product compositions. More information, including steady-state profiles along the column, is available over the internet.

This distillation process has been used as an illustrative example throughout the book, and so to avoid unnecessary repetition we will simply summarize what has been done and refer to the many exercises and examples for more details.

Remark 1 The complete linear distillation column model with 4 inputs (L, V, D, B), 4 outputs (y_D, x_B, M_D, M_B), 2 disturbances (F, z_F) and 82 states is available over the internet. The states are the mole fractions and liquid holdups on each of the 41 stages. By closing the two level loops (M_D and M_B) this model may be used to generate the model for any configuration (LV, DV, etc.). The MATLAB commands for generating the LV-, DV- and DB-configurations are given in Table 12.3.

Table 12.3: **MATLAB program for generating model of various distillation configurations**

```
% Uses MATLAB Mu toolbox
% G4: State-space model (4 inputs, 2 disturbances, 4 outputs, 82 states)
% Level controllers using D and B (P-controllers; bandwidth = 10 rad/min):
Kd = 10; Kb = 10;
% Now generate the LV-configuration from G4 using sysic:
systemnames = 'G4 Kd Kb';
inputvar = '[L(1); V(1); d(2)]';
outputvar = '[G4(1);G4(2)]';
input_to_G4 = '[L; V; Kd; Kb; d ]';
input_to_Kd = '[G4(3)]';
input_to_Kb = '[G4(4)]';
sysoutname ='Glv';
cleanupsysic='yes'; sysic;
%
% Modifications needed to generate DV-configuration:
Kl = 10; Kb = 10;
systemnames = 'G4 Kl Kb';
inputvar = '[D(1); V(1); d(2)]';
input_to_G4 = '[Kl; V; D; Kb; d ]';
input_to_Kl = '[G4(3)]';
input_to_Kb = '[G4(4)]';
sysoutname ='Gdv';
%
% Modifications needed to generate DB-configuration:
Kl = 10; Kv = 10;
systemnames = 'G4 Kl Kv';
inputvar = '[D(1); B(1); d(2)]';
input_to_G4 = '[Kl; Kv; D; B; d ]';
input_to_Kl = '[G4(3)]';
input_to_Kv = '[G4(4)]';
sysoutname ='Gdb';
```

Remark 2 A 5 state LV-model, obtained by model reducing the above model, is given on page 504. This model is also available over the internet.

12.4.1 Idealized LV-model

The following idealized model of the distillation process, originally from Skogestad et al. (1988), has been used in examples throughout the book:

$$G(s) = \frac{1}{75s+1}\begin{bmatrix} 87.8 & -86.4 \\ 108.2 & -109.6 \end{bmatrix} \tag{12.17}$$

The inputs are the reflux (L) and boilup (V), and the controlled outputs are the top and bottom product compositions (y_D and x_B). This is a very crude model of the

distillation process, but it provides an excellent example of an ill-conditioned process where control is difficult, primarily due to the presence of input uncertainty.

We refer the reader to the following places in the book where the model (12.17) is used:

Example 3.5 (page 75): SVD-analysis. The singular values are plotted as a function of frequency in Figure 3.6(b) on page 77.

Example 3.6 (page 76): Discussion of the physics of the process and the interpretation of directions.

Example 3.11 (page 89): The condition number, $\gamma(G)$, is 141.7, and the $1,1$-element of the RGA, $\lambda_{11}(G)$, is 35.1 (at all frequencies).

Motivating Example No. 2 (page 93): Introduction to robustness problems with inverse-based controller using simulation with 20% input uncertainty.

Exercise 3.7 (page 96): Design of robust SVD-controller.

Exercise 3.8 (page 96): Combined input and output uncertainty for inverse-based controller.

Exercise 3.9 (page 97): Attempt to "robustify" an inverse-based design using McFarlane-Glover $\mathcal{H}_\infty$ loop-shaping procedure.

Example 6.5 (page 232): Magnitude of inputs for rejecting disturbances (in feed rate and feed composition) at steady state.

Example 6.6 (page 240): Sensitivity to input uncertainty with feedforward control (RGA).

Example 6.7 (page 241): Sensitivity to input uncertainty with inverse-based controller, sensitivity peak (RGA).

Example 6.11 (page 245): Sensitivity to element-by-element uncertainty (relevant for identification).

Example 8.1 (page 296): Coupling between uncertainty in transfer function elements.

Example in Section 8.11.3 (page 333): μ for robust performance which explains poor performance in Motivating Example No. 2.

Example in Section 8.12.4 (page 341): Design of μ-optimal controller using DK-iteration.

The model in (12.17) has also been the basis for two benchmark problems.

Original benchmark problem. The original control problem was formulated by Skogestad et al. (1988) as a bound on the weighted sensitivity with frequency-bounded input uncertainty. The optimal solution to this problem is provided by the one degree-of-freedom μ-optimal controller given in the example in Section 8.12.4 where a peak μ-value of 0.974 (remark 1 on page 1) was obtained.

CDC benchmark problem. The original problem formulation is unrealistic in that there is no bound on the input magnitudes. Furthermore, the bounds on performance and uncertainty are given in the frequency domain (in terms of weighted $\mathcal{H}_\infty$ norm), whereas many engineers feel that time domain specifications are more realistic. Limebeer (1991) therefore suggested the following CDC-specifications. The set of plants Π is defined by

$$\widetilde{G}(s) = \frac{1}{75s+1}\begin{bmatrix} 0.878 & -0.864 \\ 1.082 & -1.096 \end{bmatrix}\begin{bmatrix} k_1 e^{-\theta_1 s} & 0 \\ 0 & k_2 e^{-\theta_2 s} \end{bmatrix}$$
$$k_i \in [\,0.8 \quad 1.2\,], \quad \theta_i \in [\,0 \quad 1.0\,] \tag{12.18}$$

In physical terms this means 20% gain uncertainty and up to 1 minute delay in each input channel. The specification is to achieve for for every plant $\widetilde{G} \in \Pi$:

S1: Closed-loop stability.

S2: For a unit step demand in channel 1 at $t = 0$ the plant output y_1 (tracking) and y_2 (interaction) should satisfy:

- $y_1(t) \geq 0.9$ for all $t \geq 30$ min
- $y_1(t) \leq 1.1$ for all t
- $0.99 \leq y_1(\infty) \leq 1.01$
- $y_1(t) \leq 0.5$ for all t
- $-0.01 \leq y_2(\infty) \leq 0.01$

The same corresponding requirements hold for a unit step demand in channel 2.

S3: $\bar{\sigma}(K_y \widetilde{S}) < 0.316, \ \forall \omega$

S4: $\bar{\sigma}(\widetilde{G} K_y) < 1$ for $\omega \geq 150$

Note that a two degrees-of-freedom controller may be used and K_y then refers to the feedback plant of the controller. In practice, specification S4 is indirectly satisfied by S3. Note that the uncertainty description $G_p = G(I + \omega_I \Delta_I)$ with $w_I = \frac{s+0.2}{0.5s+1}$ (as used in the examples in the book) only allows for about 0.9 minute time delay error. To get a weight $w_I(s)$ which includes the uncertainty in (12.18) we may use the procedure described on 268, equations (7.26) or (7.27) with $r_k = 0.2$ and $\theta_{\max} = 1$.

Several designs have been presented which satisfy the specifications for the CDC-problem in (12.18). For example, a two degrees-of-freedom $\mathcal{H}_\infty$ loop-shaping design is given by Limebeer et al. (1993), and an extension of this by Whidborne et al. (1994). A two degrees-of-freedom μ-optimal design is presented by Lundström et al. (1999).

12.4.2 Detailed LV-model

In the book we have also used a 5 state dynamic model of the distillation process which includes liquid flow dynamics (in addition to the composition dynamics) as

well as disturbances. This 5 state model was obtained from model reduction of the detailed model with 82 states. The steady-state gains for the two disturbances are given in (10.75).

The 5-state model is similar to (12.17) at low frequencies, but the model is much less interactive at higher frequencies. The physical reason for this is that the liquid flow dynamics decouple the response and make $G(j\omega)$ upper triangular at higher frequencies. The effect is illustrated in Figure 12.16 where we show the singular values and the magnitudes of the RGA-elements as functions of frequency. As a comparison, the RGA element $\lambda_{11}(G) = 35.1$ at all frequencies (and not just at steady-state) for the simplified model in (12.17). The implication is that control at crossover frequencies is easier than expected from the simplified model (12.17).

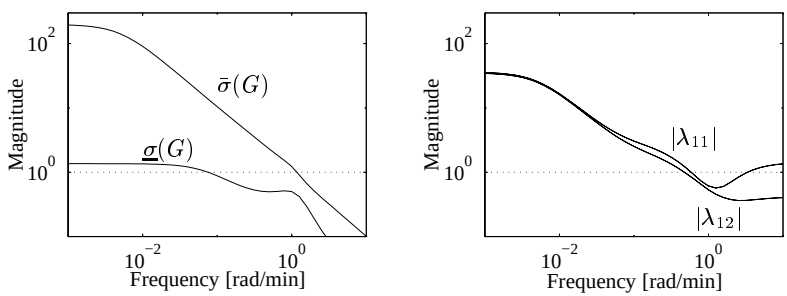

Figure 12.16: Detailed 5-state model of distillation column

Applications based on the 5 state model are found in:

*Example 10.7 (page 437)***:** Controllability analysis of partial control and feedforward control.

*Example in Section 10.10 (page 455)***:** Controllability analysis of decentralized control.

Details on the 5 state model. A state-space realization is

$$G(s) \stackrel{s}{=} \left[\begin{array}{c|c} A & B \\ \hline C & 0 \end{array}\right], \quad G_d(s) \stackrel{s}{=} \left[\begin{array}{c|c} A & B_d \\ \hline C & 0 \end{array}\right] \tag{12.19}$$

where

$$A = \begin{bmatrix} -.005131 & 0 & 0 & 0 & 0 \\ 0 & -.07366 & 0 & 0 & 0 \\ 0 & 0 & -.1829 & 0 & 0 \\ 0 & 0 & 0 & -.4620 & .9895 \\ 0 & 0 & 0 & -.9895 & -.4620 \end{bmatrix}, \quad B = \begin{bmatrix} -.629 & .624 \\ .055 & -.172 \\ .030 & -.108 \\ -.186 & -.139 \\ -1.23 & -.056 \end{bmatrix}$$

$$C = \begin{bmatrix} -.7223 & -.5170 & .3386 & -.1633 & .1121 \\ -.8913 & .4728 & .9876 & .8425 & .2186 \end{bmatrix}, \qquad B_d = \begin{bmatrix} -0.062 & -0.067 \\ 0.131 & 0.040 \\ 0.022 & -0.106 \\ -0.188 & 0.027 \\ -0.045 & 0.014 \end{bmatrix}$$

Scaling. The model is scaled such that a magnitude of 1 corresponds to the following: 0.01 mole fraction units for each output (y_D and x_B), the nominal feed flowrate for the two inputs (L and V) and a 20% change for each disturbance (feed rate F and feed composition z_F). Notice that the steady-state gains computed with this model are slightly different from the ones used in the examples.

Remark. A similar dynamic LV-model, but with 8 states, is given by Green and Limebeer (1995), who also design an $\mathcal{H}_\infty$ loop-shaping controller.

Exercise 12.1 *Repeat the μ-optimal design based on DK-iteration in Section 8.12.4 using the model (12.19).*

12.4.3 Idealized DV-model

Finally, we have also made use of an idealized model for the DV-configuration:

$$G(s) = \frac{1}{75s+1} \begin{bmatrix} -87.8 & 1.4 \\ -108.2 & -1.4 \end{bmatrix} \tag{12.20}$$

In this case the condition number $\gamma(G) = 70.8$ is still large, but the RGA elements are small (about 0.5).

Example 6.8 (page 242) Bounds on the sensitivity peak show that an inverse-based controller is robust with respect to diagonal input uncertainty.

Example 8.9 (page 323): μ for robust stability with a diagonal controller is computed. The difference between diagonal and full-block input uncertainty is significant.

Remark. In practice, the DV-configuration may not be as favourable as indicated by these examples, because the level controller at the top of the column is not perfect as was assumed when deriving (12.20).

12.4.4 Further distillation case studies

The full distillation model, which is available over the internet, may form the basis for several case studies (projects). These could include input-output controllability analysis, controller design, robustness analysis, and closed-loop simulation. The following cases may be considered:

1. Model with 4 inputs and 4 outputs
2. LV-configuration (studied extensively in this book)
3. DV-configuration (see previous page)
4. DB-configuration (see also Exercise 6.15 page 250)

The models in the latter three cases are generated from the 4×4 model by closing two level loops (see the MATLAB file in Table 12.3) to get a partially controlled plant with 2 inputs and 2 outputs (in addition to the two disturbances).

Remark 1 For the DV- and DB-configurations the resulting model depends quite strongly on the tuning of the level loops, so one may consider separately the two cases of tight level control (e.g. $K = 10$, as in Table 12.3) or loosely tuned level control (e.g. $K = 0.2$ corresponding to a time constant of 5 min). Level control tuning may also be considered as a source of uncertainty.

Remark 2 The models do not include actuator or measurement dynamics, which may also be considered as a source of uncertainty.

12.5 Conclusion

The case studies in this chapter have served to demonstrate the usefulness and ease of application of many of the techniques discussed in the book. Realistic problems have been considered but the idea has been to illustrate the techniques rather than to provide "optimal" solutions.

For the helicopter problem, practice was obtained in the selection of weights in $\mathcal{H}_\infty$ mixed-sensitivity design, and it was seen how information about disturbances could easily be considered in the design problem.

In the aero-engine study, we applied a variety of tools to the problem of output selection and then designed a two degrees-of-freedom $\mathcal{H}_\infty$ loop-shaping controller.

The final case study was a collection of examples and exercises on the distillation process considered throughout the book. This served to illustrate the difficulties of controlling ill-conditioned plants and the adverse effects of model uncertainty. The structured singular value played an important role in the robustness analysis.

You should now be in a position to move straight to Appendix B, to complete a major project on your own and to sit the sample exam.

Good luck!